Modular Integration of Upconverting Nanocrystal–Dendrimer Composites for Folate Receptor-Specific NIR Imaging and Light-Triggered Drug Release

Pamela T. Wong, Dexin Chen, Shengzhuang Tang, Sean Yanik, Michael Payne, Jhindan Mukherjee, Alexa Coulter, Kenny Tang, Ke Tao,* Kang Sun,* James R. Baker Jr., and Seok Ki Choi*

Upconversion nanocrystals (UCNs) display near-infrared (NIR)-responsive photoluminescent properties for NIR imaging and drug delivery. The development of effective strategies for UCN integration with other complementary nanostructures for targeting and drug conjugation is highly desirable. This study reports on a core/shell-based theranostic system designed by UCN integration with a folate (FA)-conjugated dendrimer for tumor targeting and with photocaged doxorubicin as a cytotoxic agent. Two types of UCNs ($NaYF_4$:Yb/Er (or Yb/Tm); diameter = ≈50 to 54 nm) are described, each displaying distinct emission properties upon NIR (980 nm) excitation. The UCNs are surface modified through covalent attachment of photocaged doxorubicin (ONB-Dox) and a multivalent FA-conjugated polyamidoamine (PAMAM) dendrimer $G5(FA)_6$ to prepare UCN@(ONB-Dox)(G5FA). Surface plasmon resonance experiments performed with $G5(FA)_6$ dendrimer alone show nanomolar binding avidity ($K_D = 5.9 \times 10^{-9}$ M) to the folate binding protein. This dendrimer binding corresponds with selective binding and uptake of UCN@(ONB-Dox)(G5FA) by FAR-positive KB carcinoma cells in vitro. Furthermore, UCN@(ONB-Dox)(G5FA) treatment of FAR(+) KB cells inhibits cell growth in a light dependent manner. These results validate the utility of modularly integrated UCN-dendrimer nanocomposites for cell type specific NIR imaging and light-controlled drug release, thus serving as a new theranostic system.

Dr. P. T. Wong, S. Tang, S. Yanik, M. Payne,
Dr. J. Mukherjee, A. Coulter, K. Tang,
Prof. J. R. Baker Jr., Prof. S. K. Choi
Michigan Nanotechnology Institute
for Medicine and Biological Sciences
Department of Internal Medicine
University of Michigan Medical School
Ann Arbor, MI 48109, USA
E-mail: skchoi@umich.edu

D. Chen, Prof. K. Tao, Prof. K. Sun
State Key Laboratory of Metal Matrix Composites
School of Materials Science and Engineering
Shanghai Jiao Tong University
Shanghai 200240, P. R. China
E-mail: ktao@sjtu.edu.cn; ksun@sjtu.edu.cn

1. Introduction

Rapid developments in biological nanotechnology have led to the identification of numerous types of photoluminescent nanomaterials[1] with promising applications in imaging,[1c–e,2] catalysis,[1c] and therapeutics.[1a] These include gold (Au) nanoparticles (NPs),[1d] quantum dots,[3] titanium dioxides,[1c,1e] and upconversion nanocrystals[4] (UCNs). The tailored applications of these nanomaterials are achieved typically through their surface modification or modular integration with other functionally designed NPs that bring together complementary capabilities needed for specific cell targeting and delivery of payloads.[5] In particular, modular integration of NPs with near-infrared (NIR)-excited UCNs has shown promising potential for deep-tissue imaging and controlled
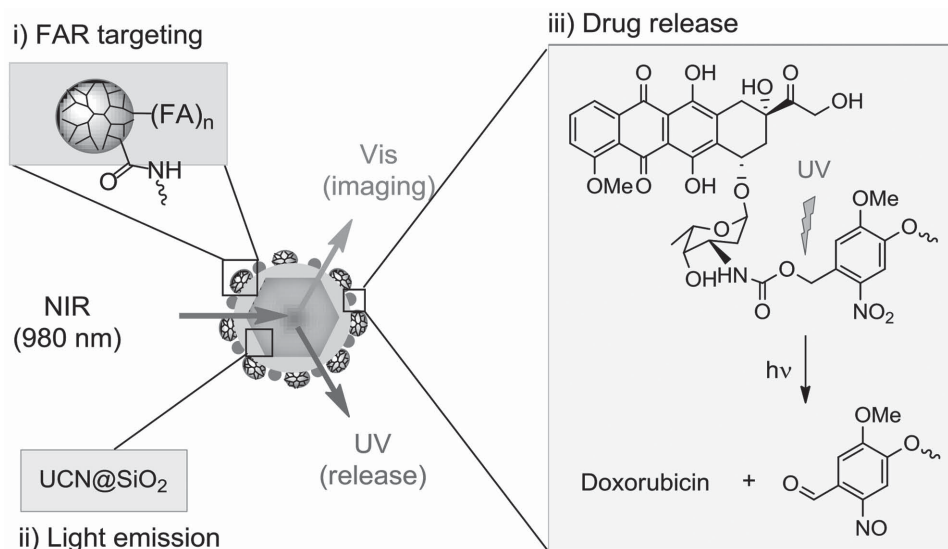
Figure 1. Modular assembly of a near-infrared (NIR)-excited upconversion nanocrystal (UCN) covalently linked with multivalent folate (FA)-conjugated dendrimer for folate receptor (FAR)-targeted cell imaging and with photocaged doxorubicin for light triggered release of doxorubicin.

payload delivery.[2,5b,6] However, despite the proven benefits imparted by such modularly integrated UCNs, the design principles of each integrated UCN nanostructure have not been addressed through a systematic assessment of the requisite design parameters. In this study, we report on the design and characterization of a novel core/shell nanostructure consisting of three functionally orthogonal modules: UCN[7] covalently coated with poly(amidoamine) (PAMAM) dendrimer[8] and photocaged doxorubicin[9] (ONB-Dox). This study addresses the key design aspects important for the efficacy of these nanocomposites in tumor receptor-targeted, temporally controlled drug delivery by assessing the effectiveness of each of the modular components in their functional roles, including cell specific targeting, imaging, and drug payload release.

As a core module, UCNs are an emerging class of photoluminescent nanostructures made of host materials such as $NaYF_4$ doped with lanthanide ions (Yb, Er, Tm, and Nd).[7,10] These UCNs are excited by NIR light (980, 800 nm)[10e] and have the unique photophysical ability to convert the absorbed NIR to shorter visible (vis) and ultraviolet (UV) light with excellent photostability and brightness.[5b,7b,10d,e] Thus, the incorporation of UCNs offers two primary advantages to modular applications. First, the NIR-excited UCN core allows for sustained tracking of tumor cells due to the lack of photobleaching which commonly limits the utility of organic fluorophores. Furthermore, NIR radiation can penetrate significantly deeper into tissue than UV radiation or visible light which is used for photodynamic therapy (PDT).[6b,c] Together, these properties make UCNs highly valuable for use in *in vivo* imaging studies.[2,5b,6e,11] Second, UV emission from the UCN core upon excitation by NIR light can be harnessed to trigger the release or activation of a conjugated payload through a photochemical mechanism.[5g,6a–d,12] The effectiveness of such modular applications of UCNs has been demonstrated in the generation of reactive oxygen species (ROS) for photodynamic therapy (PDT),[6b,c] as well

as for the release of entrapped or attached guest molecules (cisplatin,[5d] Dox,[12b,13] bovine serum albumin[5g]) and activation of photocaged molecules (platinum agent,[14] siRNA payload,[6d,15] FA ligand[6a]).

As a shell module, a fifth generation (G5) PAMAM dendrimer is coated onto the UCN surface and is responsible for the specific targeting of the composite to a tumor cell. The G5 dendrimer is the prototype of dendritic polymers. It is characterized by a globular shape (diameter = 5.4 nm)[8,16] consisting of a large number of amine-terminated branches (n_{theor} = 124), each chemically amenable to ligand or drug conjugation in a predefined orientation with conformational flexibility. Surface modification of the dendrimer with multiple targeting ligands offers the added advantage of multivalent binding,[17] allowing for extremely tight and selective adsorption to target receptors on the cell surface. Together, these properties make the G5 dendrimer an ideal platform for cell targeting.[18] The use of G5 dendrimers for targeting cancer biomarkers including folate receptor-α (FAR_α),[18a,b,d] riboflavin (RF) receptor,[5f,19] $\alpha_v\beta_3$ integrin,[20] and prostate-specific membrane antigen (PSMA[21]) has been studied extensively. Thus, the G5 dendrimer has been established as one of the most effective NPs[18b,18d,21b,22] for tumor-targeted delivery of genes[19c,20b,23] and therapeutic payloads.[18a,d,21a,24]

The present study incorporates these two nanoparticle modules in combination with photocaged doxorubicin as an anticancer therapeutic agent to generate a novel core/shell nanostructure, UCN@(ONB-Dox)(G5FA), which refers to a UCN core coated with a FA-conjugated G5 dendrimer G5(FA) and linked to a photocaged Dox[9] molecule (**Figure 1**). We designed two types of NIR-excited UCNs, one with the ability to emit vis light (540, 650 nm) suitable for imaging, and the other with the ability to emit UV light (340–360 nm) for controlled drug release. The modular nanostructure also carries a drug payload through covalent attachment to the UCN core, rather than to the dendrimer shell—the latter of which has been used in our earlier

methods for dendrimer-based drug delivery.[9,18a,25] The rationale for this site of drug conjugation relates to receptor binding avidity and drug release kinetics which are described below. However, FA was attached to the dendrimer shell because of its well validated platform capacity for tight and selective FAR binding via multivalency,[18c] and also because of the greater surface accessibility of FAR to the FA on the dendrimer as compared to presentation on the inner UCN surface. This study evaluates the design principles involved in generating and optimizing a series of UCN@(G5FA) and UCN@(ONB-Dox)(G5FA) nanostructures, and demonstrates their effectiveness with regards to FAR-specific cell binding, NIR-based optical detection, and light controlled cytotoxicity. The findings of these studies provide important insights into the modular design of UCN-based core/shell nanostructures and their relationship with the biological activity of the nanoparticle, allowing for rational optimization of design components.

2. Results and Discussion

2.1. Synthesis of UCNs

A number of methods have been developed for UCN synthesis, each with variations in the reaction condition or approach.[4a,6e–h,26] We applied a hot injection method[7b] for synthesizing two types of UCN_x ($x = 1, 2$) which display distinct upconversion properties (**Figure 2**). While each of these is excited by NIR light absorption ($\lambda_{abs} = 980$ nm), the first type of UCN, UCN_1, was designed to emit light in the vis range, while the second type of UCN, UCN_2, was designed to emit light at shorter UV–vis wavelengths. First, we synthesized UCN type 1 ($UCN_1 = NaYF_4$: 20% Yb/2% Er) by the cothermolysis (290–330 °C) of CF_3COONa and $(CF_3COO)_3Re$, (Re = Y, Yb, Er; Y:Yb:Er = 1.0:0.26:0.026) with oleic acid and sodium oleate as mixed ligands as described elsewhere.[7b] This method also allowed us to vary the diameter of UCN_1 by adjusting the amount of sodium oleate added in the thermolysis process. Second, we prepared UCN type 2 ($UCN_2 = NaYF_4$: 25% Yb/0.3% Tm) in a similar manner, except a different $(CF_3COO)_3Re$ (Re = Y, Yb, Tm) mixture and ratio (Y:Yb:Tm = 1.0:0.33:0.04) was used. After preparation of the UCNs, selected UCN_1 and UCN_2, each with d = 54 or 50 nm, respectively, were surface modified by coating with a thin amine-terminated silica layer $(NH_2)SiO_2$. This modification was performed following a nonionic water-in-oil microemulsion method[27] by treatment with (3-aminopropyl)triethoxysilane (APTES) via a silanization reaction.

The size and distribution of UCNs were determined by performing transmission electron microscopy (TEM). TEM images acquired for a representative $NaYF_4$:Yb/Er sample
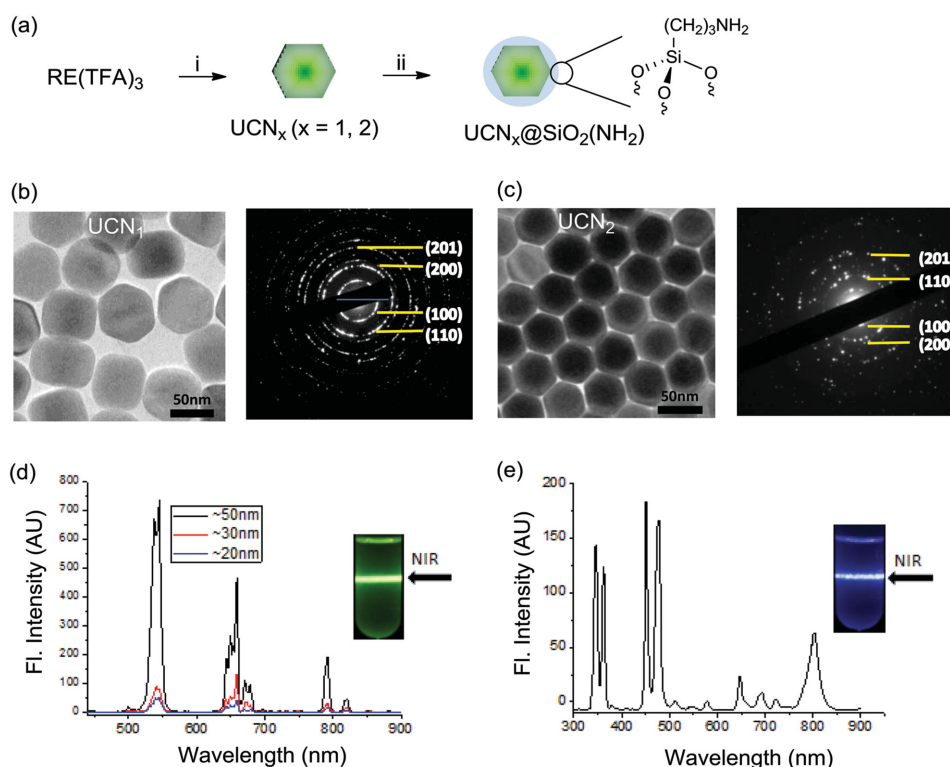
Figure 2. a) Synthetic scheme for upconversion nanocrystals UCN_x (type x = 1 or 2) and $(NH_2)SiO_2$-coated UCN_x: i) $RE(CF_3CO_2)_3$ (RE = Y, Yb and Er (for UCN_1) or Tm (for UCN_2)), CF_3CO_2Na, oleic acid sodium salt, 1-octadecene, 330 °C, 20 min; ii) (3-aminopropyl)triethoxysilane, ammonia, polyoxyethylene nonylphenylether (M_n = 441); b,c) Transmission electron microscope (TEM) images of representative UCN_1 ($NaYF_4$:20% Yb/2% Er) and UCN_2 ($NaYF_4$:25%Yb/0.3% Tm). Right: Selected area electron diffraction (SAED) patterns; d) Upconversion luminescence spectra of UCN_1 acquired by excitation at 980 nm are compared as a function of UCN diameter: black (diameter = d = 54 nm), red (d = 30 nm), and blue (d = 20 nm), each synthesized individually; e) An upconversion luminescence spectrum of UCN_2 (d = 50 nm) by excitation at 980 nm. Inset: a photograph showing emission of green light (c) or faint blue light (e) by exposure of UCN_x dispersed in chloroform (2 mg mL^{-1}) to NIR laser light (980 nm).

showed that UCN$_1$ is comprised of nanocrystals with an average diameter of ≈54 nm and a narrow size distribution (range = 45–60; Figure 2b). Some of these nanocrystals were hexagonal in shape, but others appeared less defined. However, selected area electron diffraction (SAED) patterns of NaYF$_4$:Yb/Er (right) showed diffraction rings corresponding to the (100), (110), (200), and (201) planes, indicating a hexagonal lattice. TEM analysis performed for NaYF$_4$:Yb/Tm (UCN$_2$) also showed hexagonal-shaped nanocrystals with an average diameter of ≈50 nm with a very narrow distribution (Figure 2c).

We measured the upconversion emission properties of NaYF$_4$:Yb/Er nanocrystals (UCN$_1$; d = 54 nm) by NIR excitation at 980 nm (Figure 2d). These nanocrystals showed two major emission peaks including a green band (max = 542 nm; $^4S_{3/2} \rightarrow {}^4I_{15/2}$ transition for Er^{3+}) and a red band (max = 651 nm; $^4F_{9/2} \rightarrow {}^4I_{15/2}$ transition for Er^{3+}). Fluorescence intensity at the green band was greater than at the red band. Such emission peaks and relative intensities for UCN$_1$ are consistent with the values determined for other Er, Yb-doped NaYF$_4$ nanocrystals in previous studies.[28] In addition, it is notable that the size of the UCN$_1$ has a significant impact on the efficiency of its upconversion luminescence.[6f,29] A decrease in the diameter from ≈50 to 30 or 20 nm led to a 10–15-fold reduction in emission intensity. Such size variation, however, did not change the fractional intensity ($f_{g/r}$) between the green and red bands, which remained largely similar. Thus the UCN$_1$ with a diameter of 54 nm was used for the subsequent integration steps. The upconversion luminescence properties of NaYF$_4$:Yb/Tm nanocrystals UCN$_2$ (d = 50 nm) were measured by excitation at 980 nm, which gave three emission peaks containing a UV band (340–360 nm), a blue band (450–475 nm)[30] and a broad peak at 800 nm (Figure 2e). Thus, UCN$_2$ emits a combination of vis and UV light that serves as the mechanism for UV light-controlled drug release.

2.2. Synthesis of FA-Linker

Multivalent conjugation of FA to G5 dendrimers serves as an effective strategy for tight binding of the conjugate to the FARs overexpressed (+) on certain tumor cells.[18a,b,d] Our method for FA conjugation involves prederivatization of FA with a linker terminated with a primary amine as a chemical handle for amide coupling to a carboxylic acid-terminated dendrimer molecule. We chose 2,2′-(ethylenedioxy)-bis(ethylamine) as a linker as it has a medium length that allows for conformational flexibility. The FA derivatization consisted of two steps in sequence: preactivation of FA by treatment with PyBOP ((benzotriazol-1-yloxy)tripyrrolidinophosphonium hexafluorophosphate) and 1-hydroxybenzotriazole (1-HOBt), and subsequent reaction with the diamine in situ (**Scheme 1**). After the linker derivatization, the primary amine left at the opposite end of the linker was temporarily protected as an *N*-Boc group for the convenience of purification by flash column chromatography which enabled the separation of two regioisomeric adducts of the linker at L-Glu, γ-adduct **1** (19.3%), and α-adduct (6.6%), at a ≈2.9:1

ratio. The major γ-isomer **1** was fully analyzed for its identity by standard analytical characterization methods, including ^{1}H NMR and mass spectrometry (Figure S1, Supporting Information), and the linker *N*-Boc group was deprotected by TFA treatment, yielding FA-linker **2**.

2.3. Synthesis of Photocaged Doxorubicin (ONB-Dox)

The drug module in the nanocomposite consists of a photocaged doxorubicin molecule. Photocaging refers to the temporary inactivation of a drug or ligand molecule with a molecular cage which is cleavable by light exposure.[31] This technology serves as an effective means to release or activate drug/imaging molecules through an actively controlled mechanism[22c,32] as opposed to passive release mechanisms[33] which are controlled by tumor-associated factors such as lower pH or overexpressed proteolytic enzymes. We have demonstrated the effectiveness of this drug release mechanism using a dendrimer platform in which photocaged doxorubicin (Dox)[9] or methotrexate[34] carried by an FAR-targeted G5 dendrimer is activated and released from the dendrimer in a controlled manner using UV light as the trigger. Photocaged Dox **3** was prepared by derivatization of Dox with an *ortho*-nitrobenzyl (ONB) group at its daunosamine moiety and fully characterized as described elsewhere[9] (Scheme 1, Scheme S2, Supporting Information). Removal of the linker *N*-Boc group resulted in ONB-Dox **4** which contains a free amine moiety at the linker to be used for covalent attachment to the dendrimer or UCN.

2.4. Synthesis of G5(FA)(ONB-Dox) Conjugate

Glutaric acid (GA)-modified dendrimer **6** G5(GA)[9] was employed for conjugation with FA-linker **2** alone or in combination with photocaged Dox **4** following a *N*-(3-dimethylaminopropyl)-*N*′-ethylcarbodiimide (EDC)-based amide coupling method as described elsewhere[9] (Scheme 1). First, conjugate **7** G5(FA)$_n$ (n_{mean} = 6) was prepared by covalent attachment of **2** and purified by dialysis to remove unreacted ligand and reagents present in the reaction mixture using membrane tubing (MWCO 10 kDa). Its purity (polymer homogeneity ≥94%) and structural identity were fully verified by ^{1}H NMR, UV–vis spectroscopy (λ_{max} = 354 nm, ε = 62 800 M^{-1} cm^{-1}; FA), matrix-assisted laser desorption ionization time-of-flight (MALDI-TOF) mass spectrometry (M_r = 38 600 g mol^{-1}) and gel permeation chromatography (GPC; M_p = 42 000 g mol^{-1}) (Table S1, Figures S2–S4, Supporting Information). Second, conjugate **8** G5(FA)$_n$(ONB-Dox)$_m$ was prepared similarly by coattachment of **2** and **4** to dendrimer G5(GA). The resulting conjugate **8** G5(FA)$_n$(ONB-Dox)$_m$ (n_{mean} = 6; m_{mean} = 6.9) was purified by dialysis (≥96%) and characterized by ^{1}H NMR, UV–vis spectroscopy (λ_{max} = 355 nm, ε = 163 300 M^{-1} cm^{-1} (FA); 490 nm, ε = 121 000 M^{-1} cm^{-1} (Dox)), MALDI-TOF spectrometry (M_r = 40 400 g mol^{-1}), and other methods as noted above.

Values of the valencies of the ligand (n) and the caged drug (m) were determined by Beer–Lambert analysis of
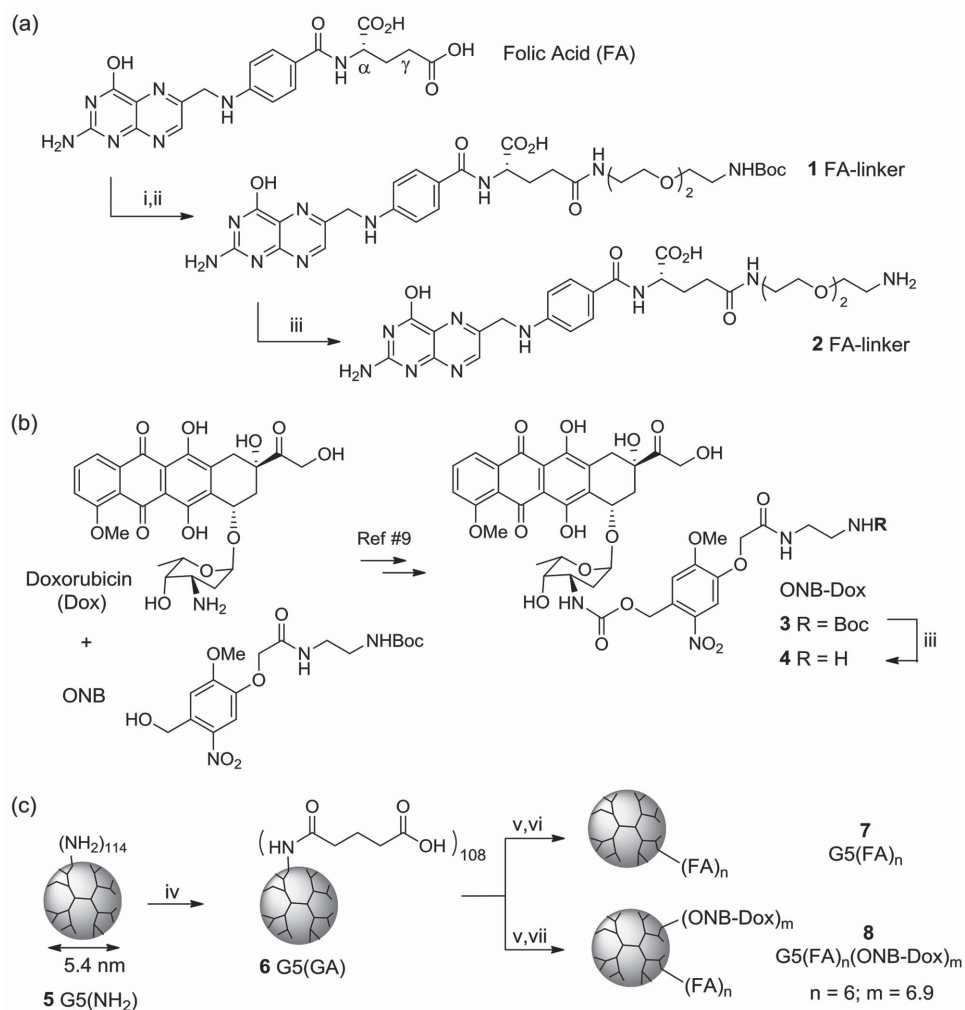
Scheme 1. Synthesis of a) folic acid (FA) derivatized with linker **2**, b) doxorubicin (Dox) caged with an ortho-nitrobenzyl (ONB) group **4**, and c) G5 dendrimer conjugates **7** and **8**.[a)]*Reagents and conditions*: i) PyBOP, HOBt, (*i*-Pr)$_2$EtN, DMSO, 1.5 h; then 2,2′-(ethylenedioxy)diethylamine (3 mol equiv), 18 h; ii) (Boc)$_2$O (7 mol equiv), 6 h; iii) CF$_3$CO$_2$H, CH$_2$Cl$_2$, 0.5 h; iv) Glutaric anhydride, Et$_3$N, MeOH; v) EDC, NHS, 4-dimethylaminopyridine, DMF, 12 h; vi) **2**, 7 h; vii) **2**, **4**, 12 h. Each reaction was performed at room temp.

UV–vis absorption (*A*) at 354 nm (FA) or 490 nm (Dox) relative to a standard calibration plot prepared by free FA or Dox and by the analysis of NMR peak integration as summarized in Table S1, Supporting Information. The two sets of values were consistent with narrow deviations lying within ±2% of their mean value.

2.5. Light-Controlled Release of Doxorubicin

Our earlier studies showed that photochemical cleavage of the ortho-nitrobenzyl (ONB; $\lambda_{max} = 340$ nm, $\varepsilon = 2750$ M^{-1} cm^{-1}) cage occurs rapidly upon exposure to UVA light (365 nm) with qunatum efficiency (Φ) of 0.29.[9,34,35] We validated the light-triggered Dox release from ONB-Dox **3** by monitoring its progress with UV–vis spectroscopy and high-performance liquid chromatography (HPLC) (**Figure 3**). Drug release was evidenced by changes in the UV–vis spectral traces of the light-exposed solutions (0.103×10^{-3} M in aq methanol) compared to unexposed solutions. They showed a gradual increase in absorption at 230–280 nm (Figure S8, Supporting Information) which is attributable to the cleavage of the ONB linker and the formation of nitrosobenzaldehyde as suggested previously.[9] HPLC analysis allowed quantitative evaluation of the release kinetics of Dox from **3**. Figure 3 shows HPLC traces acquired for the photolysed solutions as a function of exposure time. Very shortly after irradiation, a new peak appeared with a retention time (t_R) of 7.8 min which was identical to that of free Dox. The peak intensity increases rapidly as a function of UVA exposure time while the peak for ONB-Dox **3** ($t_R = 9.8$ min) decreases. Area under curve (AUC) analysis of the HPLC traces indicated that Dox release occurs efficiently with ≥85% being released within 5 min. The rapid decay of ONB-Dox had a first-order rate constant of 7.5×10^{-3} s^{-1}.

An important factor to consider is the attachment site of photocaged Dox to the UCN-dendrimer system. Dox-ONB can either be directly attached to the UCN surface or attached through conjugation to the FA-conjugated dendrimer. We first investigated whether the kinetics of Dox release from ONB-Dox is affected by dendrimer conjugation. Light-controlled Dox release from conjugate **8**
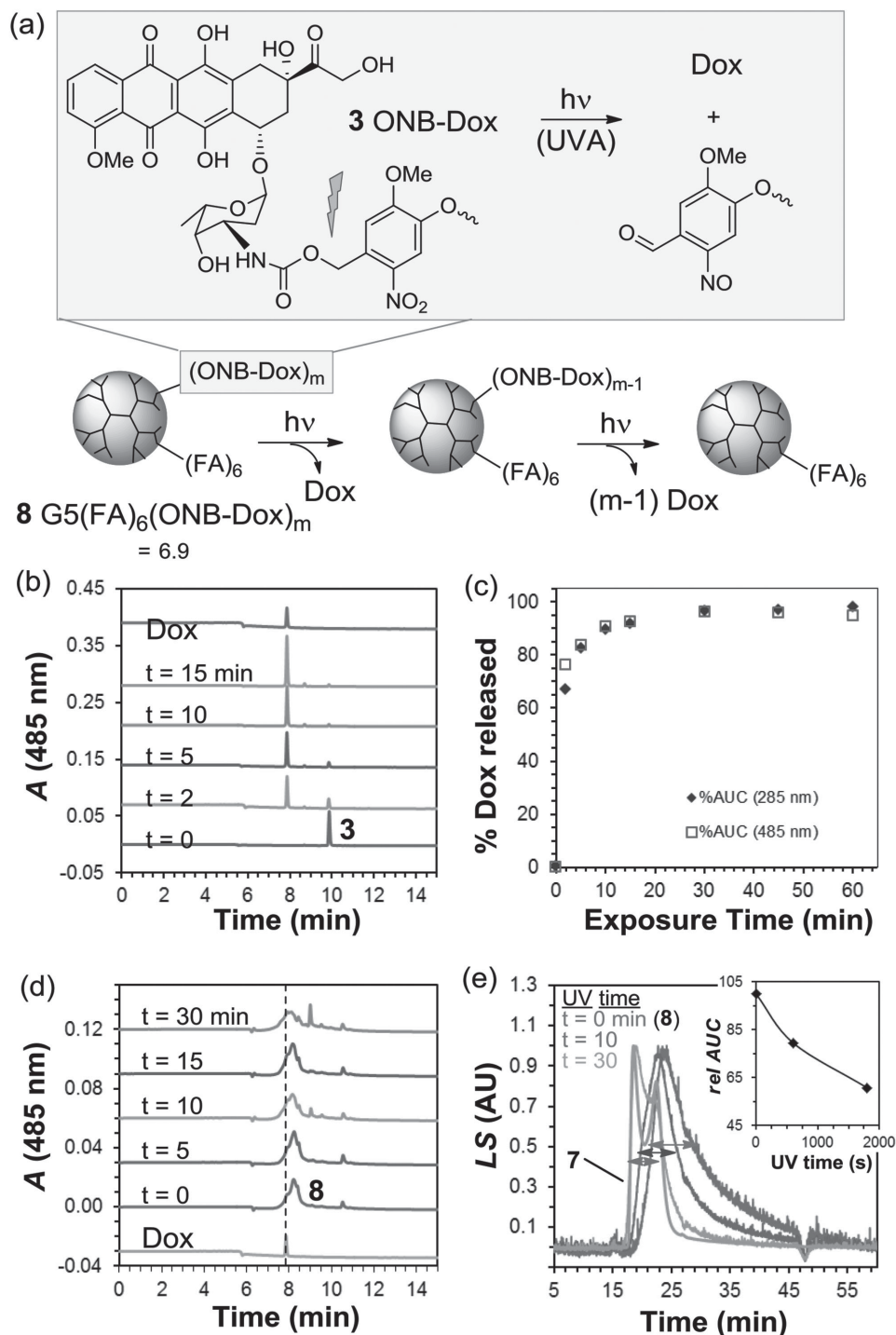
Figure 3. a) Light-controlled release of doxorubicin (Dox) from **3** ONB-Dox (top) or **8** G5 dendrimer (bottom) through the cleavage of the ortho-nitrobenzyl (ONB) cage. b) HPLC traces of **3** (0.103×10^{-3} M in 10% aq MeOH) after UVA exposure (365 nm), and c) AUC analysis of Dox release (%) vs exposure time. d) HPLC and e) GPC traces of **8** (24.8×10^{-6} M in water) after UVA treatment as a function of exposure time ($t = 0$, 10, 30 min). inset: %AUC ($t = $ exposure time) of each peak relative to AUC ($t = 0$).

G5(FA)$_6$(ONB-Dox)$_{6.9}$ in water was monitored with UV–vis spectrometry and HPLC analysis (Figure 3). Changes in the UV–vis spectral traces (Figure S8, Supporting Information) are evident, showing an increase in absorbance at 280 nm as seen with **3** ONB-Dox. Overlaid HPLC traces, each acquired after a variable length of UV exposure, showed that the broad peaks corresponding to the dendrimer species are

shifted to faster retention times over the course of UV exposure (Figure 3d). However, AUC analysis of Dox release was not attempted for these HPLC traces since the peak for free Dox ($t_R = 7.8$ min) was entirely buried within the broad dendrimer peak, and the kinetics of Dox release could not be determined for direct comparison with that of free ONB-Dox (Figure 3b).

Table 1. Kinetic parameters and equilibrium dissociation constants of FA, **7** G5(FA)$_6$ and **8** G5(FA)$_6$(ONB-Dox)$_{6.9}$ to a CM5 sensor chip immobilized with folate binding protein (FBP).

Dendrimer	k_a[a] [M^{-1} s^{-1}]	k_d[a] [s^{-1}]	K_D[b] [M]	β[c]
FA	1.5×10^3	$9.0\ (\pm 2.9) \times 10^{-3}$	5.9×10^{-6}	1.0
7 G5(FA)$_6$	1.5×10^5	$8.5\ (\pm 5.3) \times 10^{-4}$	5.9×10^{-9}	1,000 (167[d])
8 G5(FA)$_6$(ONB-Dox)$_{6.9}$	1.7×10^5	$2.8\ (\pm 0.36) \times 10^{-3}$	1.7×10^{-8}	347 (58[d])

[a]Mean value (±SD) from serially diluted concentrations ($n \geq 4$); [b]$K_D = k_d/k_a$; [c]Multivalent enhancement factor = K_D (FA)/K_D (dendrimer); [d]Valency corrected = multivalent enhancement factor/6 (= FA valency).

We expect that Dox release from conjugate **8** results in a change in the distribution of the dendrimer species. We examined this by using a novel method based on GPC analysis of the photolysed solutions. Elution profiles of the dendrimer solution before and after exposure are shown in Figure 3e. The GPC trace for **8** shows a characteristically broad peak shape (width at half height = w_h = 7.0 min), which is indicative of a wide dendrimer distribution. This is consistent with a prediction by Poissonian simulation[36] performed for **8** G5(FA)$_n$(ONB-Dox)$_m$ (n_{mean} = 6; m_{mean} = 6.9). This Poisson analysis suggests that the conjugate solution should consist of a large distribution of dendrimer species with variable conjugation ratios of the ligand and drug valency (n = 1–12; m = 2–13; Figure S4, Supporting Information). GPC traces of **8** after UV exposure for 10 and 30 min resulted in a significant decrease in the w_h to 5.9 min and 5.5 min, respectively. This narrower distribution was expected, as the heterogeneity would be reduced upon release of the attached Dox molecules (m_{mean} = 6.9 → 0). In addition, the GPC trace after 30 min exposure shows a similarity in the peak shape and t_R when compared to **7** G5(FA)$_6$, indicating the efficient release of Dox ($m_{mean} \approx 0$). AUC analysis of the GPC traces (inset, Figure 3e) was performed and the AUC decay as calculated as a first-order rate constant (2.8×10^{-4} s^{-1}) occurs at a rate ≈27-fold lower than free ONB-Dox by HPLC.

These results demonstrate that UV light serves as an effective trigger for the active control of Dox release from the ONB photocaged form. Interestingly, Dox release occurred faster from ONB-Dox **3** than from the FAR-targeted dendrimer **8** carrying the photocaged Dox. These observed differences have not been reported in literature and may be due to the presence of FA coattached to the dendrimer. The pteridine chromophore in FA has significant UV absorptivity (λ_{max} = 354 nm; ε = 62 800 M^{-1} cm^{-1}) which can effectively compete with the ONB linker for light absorption. Thus, this release study suggests that attachment of ONB-Dox to the UCN is more preferable than to the FA-conjugated dendrimer.

2.6. Binding Avidity of G5(FA) Conjugates

In our UCN-based core/shell nanostructure, the outer shell layer is comprised of the FA-conjugated dendrimer module which confers FAR-targeting properties to the nanostructure. We determined the multivalent binding avidity (K_D) of FA-conjugated dendrimers **7**, and **8** to the receptor on the surface using SPR spectroscopy. SPR is highly suited for studying multivalent receptor-ligand interactions that occur on the cell surface.[18c,37]

Folate binding protein (FBP) was immobilized on the sensor chip surface as a model receptor for FAR overexpressed on a tumor cell.[18c,19c,25] The FBP model surface was prepared following a standard EDC/NHS-based amide coupling method[18c] at a protein density of 13.1 ng mm^{-2} (response unit (RU) = 13090; Figure S6, Supporting Information). This FBP density is equivalent to a number density of ≈2.6×10^{11} FBP molecules per mm^2, comparable to the density of FAR overexpressed in several malignant cell lines including ovarian and endometrial cancers[38] (≈10^{10}–10^{11} receptor molecules per mm^2).[18c] The affinity of the immobilized FBP to FA was determined by acquiring dose-dependent sensorgrams (Figure S7a, Supporting Information). Each of the sensorgrams was fit according to a global curve fitting analysis based on a Langmuir model (1:1 binding mode) to determine the two rate constants: k_a (association) and k_d (dissociation).[39] Using these two kinetic parameters, we calculated an equilibrium dissociation constant K_D (= k_d/k_a) of 5.9×10^{-6} M (**Table 1**), comparable to those reported in the literature ($K_D = 2–5 \times 10^{-6}$ M).[18c]

SPR experiments performed with **7** G5(FA)$_6$ showed dose-dependent adsorption of the dendrimer to the FBP surface (Figure S7b, Supporting Information). Adsorption was detectable at ≤0.16×10^{-6} M, a concentration at which no binding is detectable by free FA, indicating tighter binding of the dendrimer conjugate than free FA alone. Furthermore, this conjugate dissociates much more slowly than FA. Such markedly slow desorption is consistent with earlier studies that show slow dissociation kinetics of other multivalent G5(FA)$_n$ and G5(MTX)$_n$ ($n \geq 3$; MTX = methotrexate) conjugates.[18c,24c] Global fitting analysis gave a k_d value corresponding to a ≈10-fold slower rate of desorption by **7** than FA (Table 1). This slow dissociation is a kinetic feature that contributes to the high avidity binding commonly associated with multivalent systems.[17b,17c] From this SPR analysis, the K_D value for **7** was determined as 5.9×10^{-9} M, reflecting high binding avidity with a multivalent enhancement factor of 167 (valency corrected).

Finally, the SPR experiments were performed with **8** G5(FA)$_6$(ONB-Dox)$_{6.9}$, which is identical to **7** G5(FA)$_6$ in its FA valency but in addition carries an ONB-Dox payload. This conjugate showed faster apparent dissociation than **7**. Its mean fractional desorption (= (RU$_{desorption}$/RU$_{adsorption}$) × 100%; see Figure S7, Supporting Information) calculated at the end of the dissociation phase (t = 600 s; 88 ± 2%) was larger than that of **7** G5(FA)$_6$ (t = 600 s; ≈37 ± 12%; Figure S7, Supporting
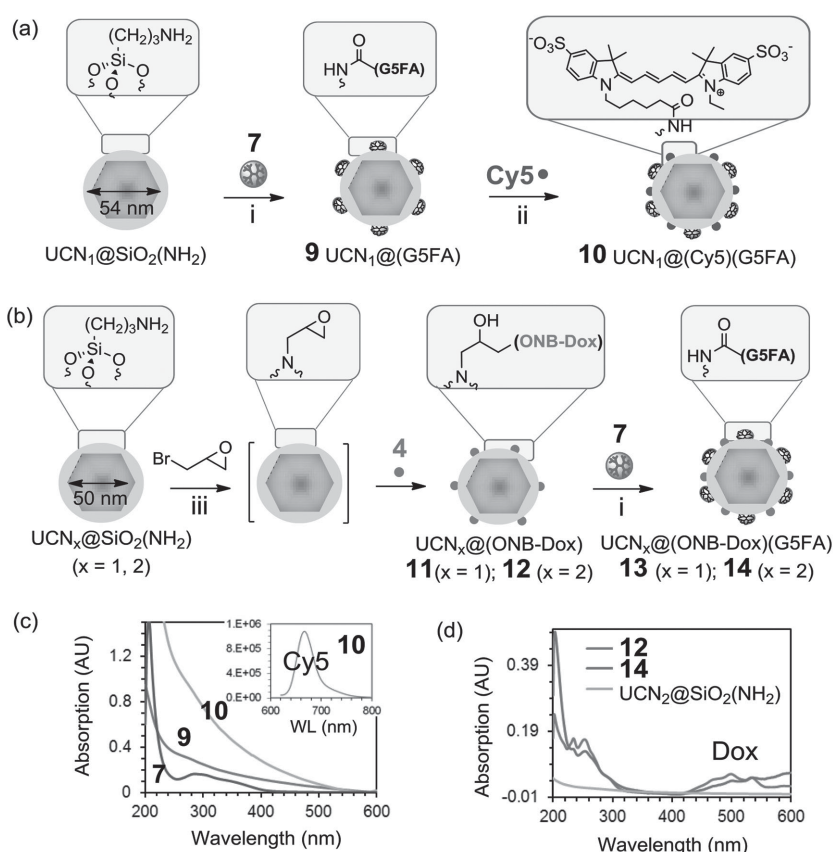
Information). Such greater desorption of **8** is largely explained by its ≈3-fold higher k_d value which leads to lower avidity with a K_D value of 1.7×10^{-8} M. We believe this reduction in avidity is caused primarily by an unfavorable steric effect[19b,40] in which the extended dendritic branches with the ONB-Dox might interfere with the optimal multivalent association between the multiple FA ligands and the receptors on the surface.

In summary, this SPR binding study demonstrated high avidity binding by FA-conjugated dendrimers to FBP receptors on the cell surface. However it was also evident that the copresence of a drug payload carried by the ligand-conjugated dendrimer compromises the targeting capability of the dendrimer carrier. These SPR results along with the slower rate of drug release observed for the dual-functional module as described above led us to rationally identify a better design approach for the UCN core/shell, in which the two separate modules, **7** G5(FA)₆ and ONB-Dox are directly attached to the UCN core independently.

Scheme 2. Synthesis of various UCN-based core/shell nanostructures, each conjugated with G5(FA)₆, Cy5 dye and/or ONB-Dox.a) a) **10** UCN1@(Cy5)(G5FA); b) **13**, **14** UCNx@(ONB-Dox)(G5FA) (x = 1, 2); c,d) UV–vis absorption spectrab),c) and fluorescence emission spectrumd) (c; inset) of selected nanostructures. a)Reagents and conditions: i) **7** G5(FA)₆, EDC, NHS, DMF, rt, 13 h; ii) Sulfo-Cy5 NHS ester, DMSO, rt; iii) epibromohydrin, MeOH, rt; then **4** ONB-Dox, rt to 45 °C. b)[**9** or **10**] = 1 mg mL⁻¹ water, [**7**] = 62.5 µg mL⁻¹ water; c)[**12** or **14**] = 1 mg mL⁻¹ MeOH; d)[**10**] = 0.25 mg mL⁻¹ MeOH; λ_{ex} = 600 nm, λ_{em} = 667 nm.

2.7. Covalent Integration of UCNs with G5(FA) and ONB-Dox

Dendrimer conjugation to the UCN was performed by amide coupling between a carboxylic acid residue in **7** G5(FA)₆ and an amine residue present in $(NH_2)SiO_2$-coated UCN_x (type x = 1, 2). It is illustrated by an EDC-based covalent attachment of **7** to UCN_1 in the synthesis of **9** UCN₁@(G5FA) (**Scheme 2**a). This dendrimer-coated UCN was further modified for imaging purposes by conjugation with a sulfo-Cy5 to yield **10** UCN₁@(Cy5)(G5FA). We attached the Cy5 dye (λ_{ex} = 600 nm, λ_{em} = 667 nm) to the nanostructure as a secondary probe for vis imaging in addition to the primary NIR imaging properties of the UCN core in order to measure cellular uptake. The UV–vis spectra of these UCN suspensions show an increase in the absorption range (≈240–400 nm) which is attributable to FA absorption (Scheme 2c). In addition, the presence of the sulfo-Cy5 label on **10** is clearly indicated by the characteristic fluorescence emission spectrum (λ_{ex} = 600 nm, λ_{em} = 667 nm; inset).

Coattachment of **7** G5(FA)₆ and **4** ONB-Dox to UCN was performed by a slightly modified method because of the need for a surface modification that allows crosslinking with amine-containing **4** (Scheme 2b). Thus, $(NH_2)SiO_2$-coated UCN was treated with epibromohydrin which converts some of its surface amine residues to amine-reactive epoxide residues. This modified UCN reacted with **4** ONB-Dox, affording drug-crosslinked **11** and **12** UCN@(ONB-Dox). UV–vis spectrometry was used to determine the fraction of ONB-Dox

attached to the UCN by analysis of the ONB-Dox solution (λ_{max} = 495 nm) before and after the conjugation reaction. The findings suggested that the weight fraction of ONB-Dox to UCN (w/w) was approximately 3.5% (**11**) and 6.5% (**12**) (the Supporting Information). In the next step, **7** G5(FA)₆ was attached by EDC-based amide coupling to **11** or **12** UCNx@(ONB-Dox), which resulted in **13** and **14** UCNx@(ONB-Dox)(G5FA) (x = 1, 2), respectively (TEM images of **13** and **14** provided in Figure S5, Supporting Information). The efficiency of this dendrimer conjugation was estimated by UV–vis analysis, indicating that ≈9% of the dendrimer added in large excess in the reaction was covalently attached. UV–vis spectra overlaid in Scheme 2d show corresponding changes in the absorption λ_{max} values and intensities indicative of surface modification of UCN with ONB-Dox (λ_{max} = 498 nm) and G5(FA)₆ (λ_{max} = 200–220 nm).

2.8. Confocal Imaging Study of UCN@(G5FA) in KB Cells In Vitro

To examine the cellular binding and uptake of the UCN nanostructures, we treated FAR-overexpressing (+) KB
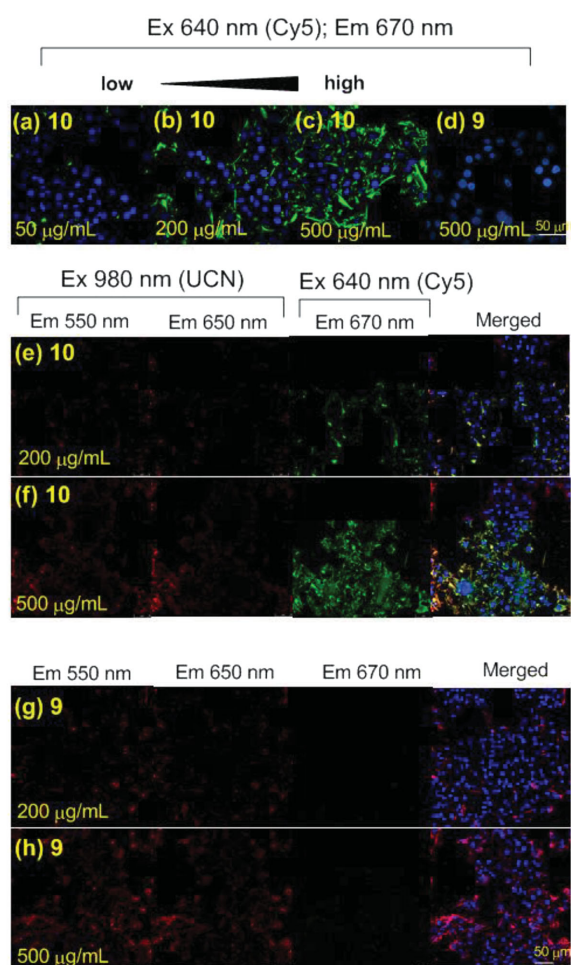
Figure 4. Cellular binding and uptake of **9** UCN$_1$@(G5FA) and **10** UCN$_1$@(Cy5)(G5FA) in FAR(+) KB cells imaged by confocal microscopy. a–d) Images of KB cells treated with **10** or **9** taken in Cy5 mode (λ_{ex} = 640 nm; λ_{em} = 670 nm). e–h) Images of KB cells treated with **10** or **9** taken in both NIR mode for imaging the UCN core (λ_{ex} = 980 nm; λ_{em} = 550 nm, 650 nm) and Cy5 mode. DAPI (blue: nuclei); UCN core (red), Cy5 (green).

tumor cells with increasing concentrations (50–500 µg mL^{-1}) of **9** UCN$_1$@(G5FA) or **10** UCN$_1$@(Cy5)(G5FA) for 2 h, and imaged the cells with confocal microscopy using two detection modes: (i) Cy5 mode (λ_{ex} = 640 nm; λ_{ex} = 670 nm) and (ii) UCN$_1$ NIR mode (λ_{ex} = 980 nm; λ_{ex} = 550, 650 nm). As shown in **Figure 4**, confocal images of the cells with **10** clearly indicated dose-dependent binding and uptake by KB cells (Figure 4a–c). No signal was detected through this Cy5 channel in cells treated with **9**, an identical nanoparticle without the Cy5 attachment, confirming that the fluorescence signal is from the Cy5 (Figure 4d).

We then imaged the treated cells in NIR mode with excitation at 980 nm and detection at 550 or 650 nm (Figure 4). The localization of FAR-targeted UCNs on the cell surface as well as intracellularly was observed under both the NIR and Cy5 imaging modes in cells treated with **10** (200 or 500 µg mL^{-1}). Merged images showed colocalization of the NIR and Cy5 signals, demonstrating the ability to image UCNs with either mode of detection (Figure 4e,f). Furthermore, UCN **9** could be detected under the NIR mode despite
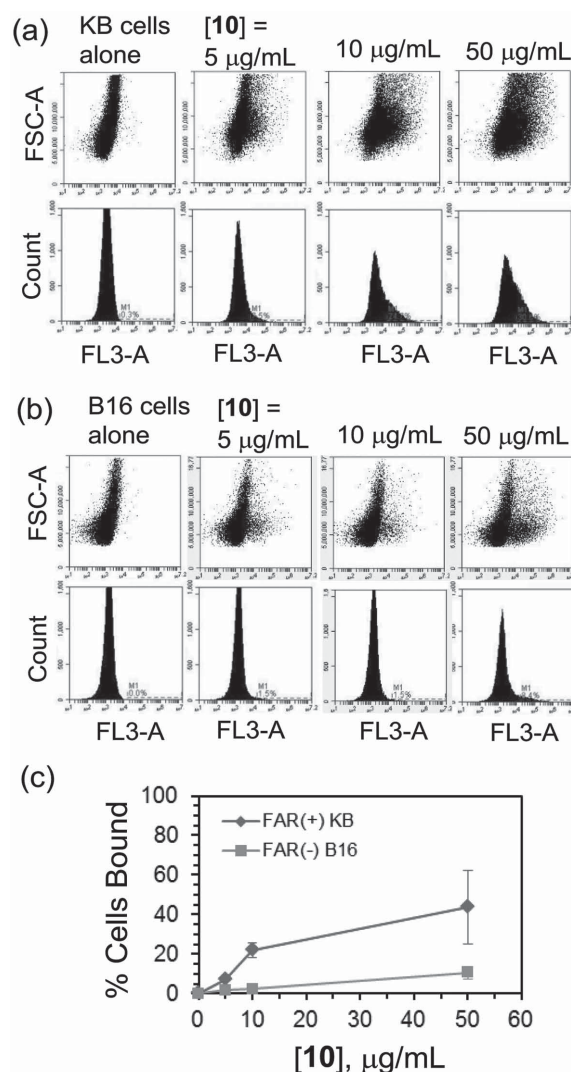

Figure 5. a,b) Flow cytometric analysis of binding and uptake of **10** UCN$_1$@(Cy5)(G5FA) by FAR(+) KB cells and FAR(–) B16 F10 cells. c) Fraction of cells with bound or internalized UCN, determined by the percentage of cells with Cy5 fluorescence (FL3) greater than that of cells alone (gate M1). Each data point represents a mean value of duplicate measurements (±SD).

the absence of the Cy5 label (Figure 4g,h). Thus, visible light-emitting UCN$_1$ serves as an effective platform for label free cellular imaging with NIR excitation.

2.9. Flow Cytometric Analysis of UCN@(G5FA) Binding and Uptake in KB Cells In Vitro

Cellular association of **10** UCN$_1$@(Cy5)(G5FA) was further investigated by flow cytometry. Two cell lines which are distinct in their FAR density were used to determine the specificity of UCN in FAR targeting: FAR(+) KB cells and FAR(–) B16-F10 cells (a mouse melanoma cell line). Cells were incubated with variable concentrations of **10** (0–50 µg mL^{-1}) for 1 h in FA-free media at 37 °C and analyzed. Histograms and fluorescence intensities (FL3 for Cy5) of gated live cells are shown in **Figure 5**. The fraction of KB cells with bound **10**

increased in a dose-dependent manner. In contrast, FAR(−) B16 cells showed only a small fraction of cells with bound UCN under the same conditions (Figure 5b). The fraction of bound cells determined at the highest concentration (50 μg mL^{-1}) was 44 ± 19% for FAR(+) KB cells compared to only 11 ± 3% for FAR(−) B16 cells. These results support the specific binding and uptake of **10** UCN$_1$@(Cy5)(G5FA) by a FAR-dependent mechanism. As evidence further supporting FAR specificity, cells were incubated with **10** (10 μg mL^{-1} UCN equivalent to ≈0.02 × 10^{-6} M FA) in the presence of free FA (50 × 10^{-6} M) to verify whether FA could competitively inhibit nanoparticle adsorption to KB cells. Addition of 50 × 10^{-6} M FA led to a decrease in the fraction of cells with bound UCN from 44% to 31%. This competitive inhibition is supportive of FAR-specific cell binding, though such a small effect is perhaps due to the weaker μM affinity of FA relative to the higher affinity of the multivalent dendrimer attached to the UCN.

FAR-specific cell binding by **10** is consistent with earlier results observed with FAR-targeted dendrimers such as G5(FA)$_{6.4}$(ONB-Dox)$_{5.9}$ and G5(MTX)$_{10}$.[9,18c,24c] The binding avidity of **10** to a FAR model surface was not measurable by SPR because of its suspension-like nature (due to low solubility in water), however we believe that such cell specificity is primarily attributable to the tight multivalent interactions between multiple G5(FA)$_6$ dendrimers in the shell layer and the cell surface receptors as suggested by the SPR study above ($K_D = 5.9 \times 10^{-9}$ M; Table 1).

2.10. Light-Controlled Cytotoxicity of UCNs Conjugated with ONB-Dox

Lastly, we evaluated the efficacy of two different types of light excitation for the controlled induction of cytotoxicity by **13** UCN$_1$@(ONB-Dox)(G5FA) or **14** UCN$_2$@(ONB-Dox)(G5FA) in FAR(+) KB cancer cells (**Figure 6**). **13** consists of 3.5% (w/w) **4** ONB-Dox:UCN conjugate and **14** consists of 6.5% (w/w) **4** ONB-Dox:UCN conjugate. We employed this cell-based assay primarily to compare the overall cytotoxicity of each UCN conjugate triggered by UV and NIR irradiation. This assay allows direct determination of the functional activity of decaged (activated) drug molecules by addressing both the release efficiency and penetration capability of each light source through cellular membranes. UV light was first validated as a reference light source for Dox release. KB cells were treated with **13** or **14** and the cell viability was determined under two different exposure conditions (Figure S9, Supporting Information): "pre-exposed 0.5 h" and "1 h exposure on cells." In the first condition ("pre-exposed 0.5 h"), the test solution alone in PBS/1% BSA (PBSB) was exposed to UV light (365 nm) for 0.5 h prior to its addition to and incubation with the cells for 1.5 h at 37 °C. In the other condition ("1 h exposure on cells"), the cells were incubated with each test solution in PBSB and the entire mixture of cells with UCN was exposed to UV light for 1 h followed by incubation at 37 °C for an additional 0.5 h. Fresh media was added to all of the treated cells to dilute the conjugate by a factor of four, and the cells were incubated for 24 h prior to
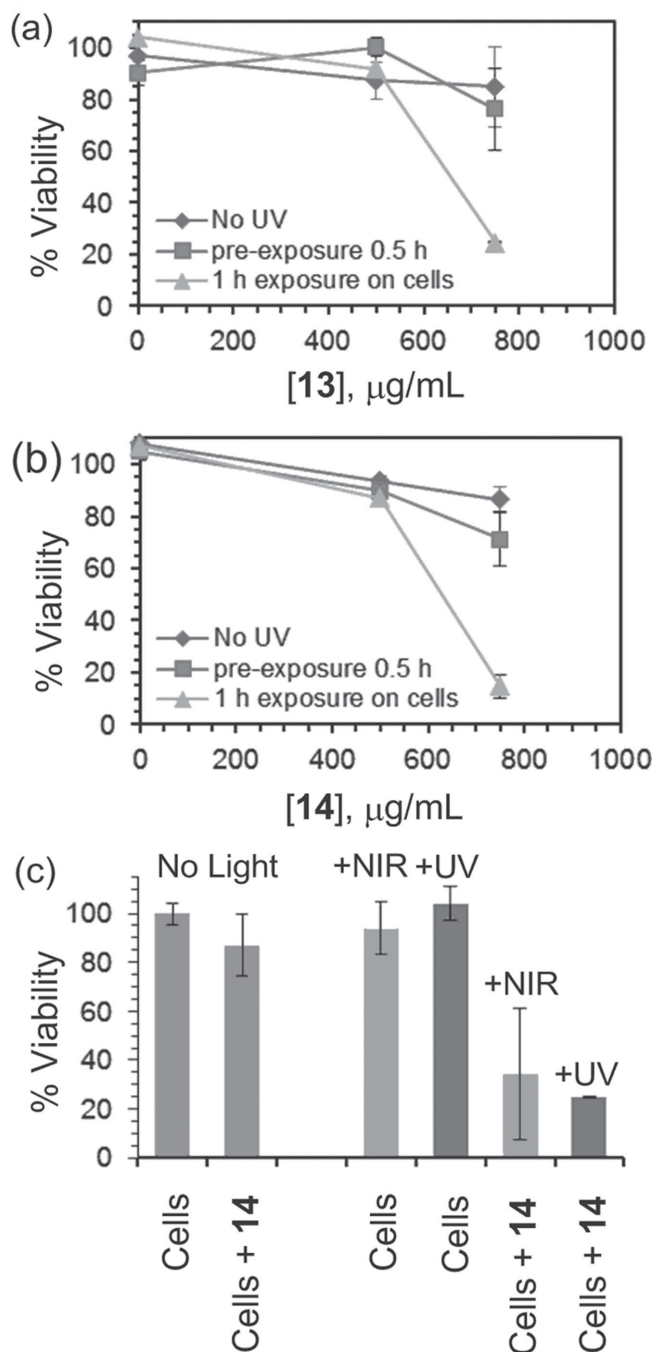

Figure 6. Light-controlled cytotoxicity of **13** UCN$_1$@(ONB-Dox)(G5FA) and **14** UCN$_2$@(ONB-Dox)(G5FA) in FAR(+) KB cancer cells. (a, b) Viability (%) of cells treated with **13** or **14** and exposed to a UV lamp (365 nm; 15 W; output = ≈3 × 10^{19} photons s^{-1}) under two different conditions as defined in the text. Each data point refers to a mean value (±SD; $n \geq 3$). c) Viability (%) of cells treated with **14** ([UCN] = 750 μg mL^{-1}), each with or without exposure to a continuous wave NIR laser (980 nm; 1 W; output = ~5 × 10^{18} photons s^{-1}) or a UV lamp for 1 h exposure on cells. Each bar represents a mean value (±SD; $n \geq 5$).

replacing the conjugate containing media with fresh media. Viability was measured after 4 d of incubation at 37 °C in this fresh media.

As shown in Figure 6a,b, The KB cells were treated with **13** or **14** suspended at two concentrations: 500 μg mL^{-1}:

equivalent [ONB-Dox] = 20×10^{-6} M (**13**), 30×10^{-6} M (**14**); 750 µg mL^{-1}: [Dox-ONB] = 37×10^{-6} M (**13**), 56×10^{-6} M (**14**). Treatment at the lower concentration was ineffective regardless of light exposure. In contrast, treatment at the higher concentration led to a marked decrease in viability and was highly dependent on the conditions of the light exposure. In particular, the "exposure on cells" condition in which the cells were incubated with the UCN prior to being exposed to UV light was the most effective in killing the cells. Similarly, the KB cells were treated with **4** ONB-Dox and **8** G5(FA)$_6$(Dox)$_{6.9}$ as positive controls under various conditions of light exposure, as summarized in Figure S10, Supporting Information. This study validated the light control of Dox release from the UCN conjugates, and also allowed us to identify a threshold nanoparticle dose for inducing cytotoxicity in KB cells in a light dependent manner.

In contrast to conjugate **13** which contains a UCN$_1$ core that only emits in the visible range, conjugate **14** consists of a UCN$_2$ core that emits UV light (λ_{em} = 345, 362 nm) upon excitation with NIR (980 nm) (Figure 2). We thus investigated whether excitation of **14** UCN$_2$@(ONB-Dox)(G5FA) with NIR could trigger drug release and subsequently result in cytotoxicity. FAR(+) KB cells were treated with 750 µg mL^{-1} the UCN conjugate and the cells were exposed to NIR radiation (980 nm; power output = 1 W) for 1 h ("1 h exposure on cells"). Figure 6c compares the effect of exposure to NIR and UV light to dark controls. Cells showed no significant decrease in viability in the presence or absence of **14** without any exposure to light excitation. Exposure to UV or NIR light for the treatment period also did not have any significant impact on cell viability. However, exposure of cells treated with **14** to NIR light led to a significant decrease in cell viability comparable to that induced by the direct cleavage of the photocaged Dox by UV triggered release.

Cytotoxicity as triggered by NIR, however, showed a wider variation (±SD) in activity. We believe this experimental error is attributable to a number of technical challenges facing the NIR exposure. First, unlike the UV release which was performed under a UV lamp, NIR release was performed by irradiation with a continuous wave (CW) NIR laser. Thus the wide variation between replicates could have been due to the lack of homogeneous excitation across each sample well due to the relatively small size of the laser beam. Second, NIR release requires an extended period of irradiation (1 h) primarily due to the low quantum yield of UV emission from UCN$_2$ as illustrated by the low intensity of its UV emission peaks relative to the intensity of UCN$_1$ visible emission (Figure 2). Despite such technical challenges that need to be addressed, we believe that this NIR release study supports the use of the UCN core as an effective way to control drug release by NIR radiation.

3. Conclusion

In summary, in this study, we employed a bottom-up approach toward the modular integration of UCN with a FAR-targeted multivalent dendrimer G5(FA)$_6$ and photocaged doxorubicin ONB-Dox. Integration of these three individually functional components into a single nanostructure could be achieved through a variety of conceivable combinations. Many design aspects fundamental to this type of UCN integration (ex. drug or targeting ligand attachment sites) have not been systematically evaluated in previous studies.[2,5b,6a–e]

The rationale for designing such composite UCN nanostructures lies in the unique optical properties conferred by the UCN cores, in which the UCN core selectively absorbs focused NIR (980 nm) light and emits UV–vis light,[5g,6a,b,d] thus serving as a light emitting nanodevice. Two UCN types were designed: UCN$_1$ (λ_{em} = 542, 651 nm) suitable for vis imaging and UCN$_2$ (λ_{em} = 340–360, 450–475 nm) suitable for light-controlled drug release. UCN$_1$@(G5FA) enabled the use of NIR imaging for sensitive, label-free detection of FAR(+) carcinoma cells. Furthermore, UCN$_2$ integration into the UCN$_2$@(ONB-Dox)(G5FA) nanocomposite allowed for effective targeted drug delivery triggered by either UV or NIR irradiation. Our approach for the controlled release of Dox is based on its temporary inactivation with a UV light-cleavable cage, an *ortho*-nitrobenzyl (ONB) group. UVA light penetrates through the skin, reaching cells in the layers of the epidermis and dermis (depth ≤0.15 mm),[41] providing a potentially spatial mechanism of drug release to tumor cells localized to the skin and vascular endothelial cells. However, the use of UV-triggered photorelease for targeting more interiorly located tumors is limited by the penetration depth of UV excitation. Integration of the photocaged drug with UCNs, however, allows for the use of a NIR excitation light source in place of UV to trigger drug release using the same UV-cleavable photocage due to the UV emission of the UCN core upon excitation with NIR. This ability to trigger drug delivery with NIR enables the use of photocontrolled drug delivery to target more interiorly localized cells, as NIR light penetrates deep into tissues (depth ≥2–3 mm) without a significant loss of transmission from absorption by water.[41] We believe that these novel NIR-excited UCN nanocomposite structures have great potential for extending the scope of imaging and drug release from UV-accessible skin cells to other tissues and inner organs of interest. Furthermore, the lower energy of NIR makes it more desirable as a treatment light source relative to UVA, which while less damaging than UVB, still has the potential to damage bystander cells upon prolonged exposure.

Two modes for structural integration of photocaged doxorubicin ONB-Dox were examined: conjugation to G5(FA)$_6$ or direct conjugation to the UCN. Our findings suggested potentially greater benefits through the direct attachment of photocaged drug to the UCN surface. Coconjugation of ONB-Dox and FA to the PAMAM dendrimer G5(FA)$_6$(ONB-Dox) resulted in lower binding avidity to the model surface for a FAR(+) cell compared to G5(FA)$_6$ perhaps due to steric interference from the bulky Dox molecule blocking FAR access to the FA ligand molecule. In the UV-mediated drug release study, Dox release occurred faster from ONB-Dox than from the dendrimer conjugated form G5(FA)$_6$(ONB-Dox). Thus, cell receptor targeting avidity and specificity as well as drug release kinetics from UCN nanocomposites appear to be highly dependent on the site of conjugation of the targeting ligand and photocaged drug payload. Considering all of these

data together, this study provides implications of significant importance to the design and screening of multifunctional UCN nanostructures for surface receptor-targeted imaging and treatment of tumor cells.

4. Experimental Section

Methods for the synthesis of UCNs, G5 PAMAM dendrimer and photocaged Dox, and analytical methods (TEM, HPLC, GPC, ^{1}H NMR, UV–vis spectrometry, MALDI-TOF mass spectrometry) are described in detail in the Supporting Information and references cited therein. Full details for other materials and methods (drug release kinetics, SPR spectroscopy, cell culture, flow cytometry, confocal microscopy) are also provided in the Supporting Information.

Supporting Information

Supporting Information is available from the Wiley Online Library or from the author.

Acknowledgements

[1] a) V. Biju, *Chem. Soc. Rev.* **2014**, *43*, 744; b) L. Cheng, C. Wang, L. Feng, K. Yang, Z. Liu, *Chem. Rev.* **2014**, *114*, 10869; c) M. Dahl, Y. Liu, Y. Yin, *Chem. Rev.* **2014**, *114*, 9853; d) N. L. Rosi, C. A. Mirkin, *Chem. Rev.* **2005**, *105*, 1547; e) X. Wu, H. Liu, J. Liu, K. N. Haley, J. A. Treadway, J. P. Larson, N. Ge, F. Peale, M. P. Bruchez, *Nat. Biotechnol.* **2003**, *21*, 41.

[2] M. Wang, C.-C. Mi, W.-X. Wang, C.-H. Liu, Y.-F. Wu, Z.-R. Xu, C.-B. Mao, S.-K. Xu, *ACS Nano* **2009**, *3*, 1580.

[3] L. A. Ponomarenko, F. Schedin, M. I. Katsnelson, R. Yang, E. W. Hill, K. S. Novoselov, A. K. Geim, *Science* **2008**, *320*, 356.

[4] a) S. Heer, K. Kömpe, H. U. Güdel, M. Haase, *Adv. Mater.* **2004**, *16*, 2102; b) X. Liu, C.-H. Yan, J. A. Capobianco, *Chem. Soc. Rev.* **2015**, *44*, 1299; c) S. Gai, C. Li, P. Yang, J. Lin, *Chem. Rev.* **2014**, *114*, 2343; d) D. Yang, P. a. Ma, Z. Hou, Z. Cheng, C. Li, J. Lin, *Chem. Soc. Rev.* **2015**, *44*, 1416.

[5] a) A. Agarwal, M. A. Mackey, M. A. El-Sayed, R. V. Bellamkonda, *ACS Nano* **2011**, *5*, 4919; b) J. Jin, Y.-J. Gu, C. W.-Y. Man, J. Cheng, Z. Xu, Y. Zhang, H. Wang, V. H.-Y. Lee, S. H. Cheng, W.-T. Wong, *ACS Nano* **2011**, *5*, 7838; c) X. Li, H. Zhou, L. Yang, G. Du, A. S. Pai-Panandiker, X. Huang, B. Yan, *Biomaterials* **2011**, *32*, 2540; d) P. a. Ma, H. Xiao, X. Li, C. Li, Y. Dai, Z. Cheng, X. Jing, J. Lin, *Adv. Mater.* **2013**, *25*, 4898; e) J. L. Vivero-Escoto, I. I. Slowing, C.-W. Wu, V. S. Y. Lin, *J. Am. Chem. Soc.* **2009**, *131*, 3462; f) A. B. Witte, A. N. Leistra, P. T. Wong, S. Bharathi, K. Refior,

[6] a) Y.-H. Chien, Y.-L. Chou, S.-W. Wang, S.-T. Hung, M.-C. Liau, Y.-J. Chao, C.-H. Su, C.-S. Yeh, *ACS Nano* **2013**, *7*, 8516; b) S. Cui, D. Yin, Y. Chen, Y. Di, H. Chen, Y. Ma, S. Achilefu, Y. Gu, *ACS Nano* **2012**, *7*, 676; c) N. M. Idris, M. K. Gnanasammandhan, J. Zhang, P. C. Ho, R. Mahendran, Y. Zhang, *Nat. Med. (N. Y., NY, U. S.)* **2012**, *18*, 1580; d) M. K. G. Jayakumar, N. M. Idris, Y. Zhang, *Proc. Natl. Acad. Sci. USA* **2012**, *109*, 8483; e) Y. Sun, X. Zhu, J. Peng, F. Li, *ACS Nano* **2013**, *7*, 11290; f) F. Wang, X. Liu, *Acc. Chem. Res.* **2014**, *47*, 1378; g) Y.-F. Wang, G.-Y. Liu, L.-D. Sun, J.-W. Xiao, J.-C. Zhou, C.-H. Yan, *ACS Nano* **2013**, *7*, 7200; h) S. Han, R. Deng, X. Xie, X. Liu, *Angew. Chem. Int. Ed.* **2014**, *53*, 11702; i) Y. Dai, H. Xiao, J. Liu, Q. Yuan, P. a. Ma, D. Yang, C. Li, Z. Cheng, Z. Hou, P. Yang, J. Lin, *J. Am. Chem. Soc.* **2013**, *135*, 18920; j) S. Gai, P. Yang, C. Li, W. Wang, Y. Dai, N. Niu, J. Lin, *Adv. Funct. Mater.* **2010**, *20*, 1166.

[7] a) Y. Sui, K. Tao, Q. Tian, K. Sun, *J. Phys. Chem. C* **2011**, *116*, 1732; b) Q. Tian, K. Tao, W. Li, K. Sun, *J. Phys. Chem. C* **2011**, *115*, 22886.

[8] D. A. Tomalia, A. M. Naylor, I. William, A. Goddard, *Angew. Chem. Int. Ed.* **1990**, *29*, 138.

[9] S. K. Choi, T. Thomas, M. Li, A. Kotlyar, A. Desai, J. R. Baker Jr., *Chem. Commun.* **2010**, *46*, 2632.

[10] a) J.-C. Boyer, F. Vetrone, L. A. Cuccia, J. A. Capobianco, *J. Am. Chem. Soc.* **2006**, *128*, 7444; b) G. Chen, H. Qiu, P. N. Prasad, X. Chen, *Chem. Rev.* **2014**, *114*, 5161; c) M. Haase, H. Schäfer, *Angew. Chem. Int. Ed.* **2011**, *50*, 5808; d) F. Wang, X. Liu, *Chem. Soc. Rev.* **2009**, *38*, 976; e) J. Shen, G. Chen, A.-M. Vu, W. Fan, O. S. Bilsel, C.-C. Chang, G. Han, *Adv. Opt. Mater.* **2013**, *1*, 644.

[11] Y. Yang, Q. Shao, R. Deng, C. Wang, X. Teng, K. Cheng, Z. Cheng, L. Huang, Z. Liu, X. Liu, B. Xing, *Angew. Chem. Int. Ed.* **2012**, *51*, 3125.

[12] a) J. Shen, G. Chen, T. Y. Ohulchanskyy, S. J. Kesseli, S. Buchholz, Z. Li, P. N. Prasad, G. Han, *Small* **2013**, *9*, 3213; b) Y. Yang, B. Velmurugan, X. Liu, B. Xing, *Small* **2013**, *9*, 2937.

[13] M. M. Dcona, Q. Yu, J. A. Capobianco, M. C. T. Hartman, *Chem. Commun.* **2015**, *51*, 8477.

[14] Y. Min, J. Li, F. Liu, E. K. L. Yeow, B. Xing, *Angew. Chem. Int. Ed.* **2014**, *53*, 1012.

[15] Y. Yang, F. Liu, X. Liu, B. Xing, *Nanoscale* **2013**, *5*, 231.

[16] D. A. Tomalia, H. Baker, J. Dewald, M. Hall, G. Kallos, S. Martin, J. Roeck, J. Ryder, P. Smith, *Polym. J.* **1985**, *17*, 117.

[17] a) C. Fasting, C. A. Schalley, M. Weber, O. Seitz, S. Hecht, B. Koksch, J. Dernedde, C. Graf, E.-W. Knapp, R. Haag, *Angew. Chem. Int. Ed.* **2012**, *51*, 10472; b) L. L. Kiessling, J. E. Gestwicki, L. E. Strong, *Angew. Chem. Int. Ed.* **2006**, *45*, 2348; c) M. Mammen, S. K. Choi, G. M. Whitesides, *Angew. Chem. Int. Ed.* **1998**, *37*, 2754.

[18] a) J. F. Kukowska-Latallo, K. A. Candido, Z. Cao, S. S. Nigavekar, I. J. Majoros, T. P. Thomas, L. P. Balogh, M. K. Khan, J. R. Baker Jr., *Cancer Res.* **2005**, *65*, 5317; b) I. J. Majoros, C. R. Williams, A. Becker, J. R. Baker Jr., *Wiley Interdiscip. Rev.: Nanomed. Nanobiotechnol.* **2009**, *1*, 502; c) J. E. Silpe, M. Sumit, T. P. Thomas, B. Huang, A. Kotlyar, M. A. van Dongen, M. M. Banaszak Holl, B. G. Orr, S. K. Choi, *ACS Chem. Biol.* **2013**, *8*, 2063; d) J. Zhu, X. Shi, *J. Mater. Chem. B* **2013**, *1*, 4199.

[19] a) T. P. Thomas, S. K. Choi, M.-H. Li, A. Kotlyar, J. R. Baker Jr., *Bioorg. Med. Chem. Lett.* **2010**, *20*, 5191; b) A. B. Witte, C. M. Timmer, J. J. Gam, S. K. Choi, M. M. Banaszak Holl, B. G. Orr, J. R. Baker, K. Sinniah, *Biomacromolecules* **2012**, *13*, 507; c) P. T. Wong, K. Tang, A. Coulter, S. Tang, J. R. Baker, S. K. Choi, *Biomacromolecules* **2014**, *15*, 4134.

[20] a) C. A. Boswell, P. K. Eck, C. A. S. Regino, M. Bernardo, K. J. Wong, D. E. Milenic, P. L. Choyke, M. W. Brechbiel, *Mol. Pharmaceutics* **2008**, *5*, 527; b) L. Kong, C. S. Alves, W. Hou, J. Qiu, H. Möhwald,

H. Tomás, X. Shi, *ACS Appl. Mater. Interfaces* **2015**, *7*, 4833; c) R. Shukla, T. P. Thomas, J. Peters, A. Kotlyar, A. Myc, J. R. Baker Jr., *Chem. Commun.* **2005**, 5739.

[21] a) B. Huang, J. Otis, M. Joice, A. Kotlyar, T. P. Thomas, *Biomacromolecules* **2014**, *15*, 915; b) S. H. Medina, M. E. H. El-Sayed, *Chem. Rev.* **2009**, *109*, 3141.

[22] a) W. T. Al-Jamal, K. Kostarelos, *Acc. Chem. Res.* **2011**, *44*, 1094; b) S. M. Janib, A. S. Moses, J. A. MacKay, *Adv. Drug Delivery Rev.* **2010**, *62*, 1052; c) M. R. Molla, P. Rangadurai, G. M. Pavan, S. Thayumanavan, *Nanoscale* **2015**, *7*, 3817; d) D. Peer, J. M. Karp, S. Hong, O. C. Farokhzad, R. Margalit, R. Langer, *Nat. Nanotechnol.* **2007**, *2*, 751.

[23] T. Xiao, W. Hou, X. Cao, S. Wen, M. Shen, X. Shi, *Biomater. Sci.* **2013**, *1*, 1172.

[24] a) E. N. Cline, M.-H. Li, S. K. Choi, J. F. Herbstman, N. Kaul, E. Meyhöfer, G. Skiniotis, J. R. Baker, R. G. Larson, N. G. Walter, *Biomacromolecules* **2013**, *14*, 654; b) I. J. Majoros, A. Myc, T. Thomas, C. B. Mehta, J. R. Baker, *Biomacromolecules* **2006**, *7*, 572; c) T. P. Thomas, B. Huang, S. K. Choi, J. E. Silpe, A. Kotlyar, A. M. Desai, J. Gam, M. Joice, J. R. Baker Jr., *Mol. Pharmaceutics* **2012**, *9*, 2669.

[25] M.-H. Li, S. K. Choi, T. P. Thomas, A. Desai, K.-H. Lee, A. Kotlyar, M. M. Banaszak Holl, J. R. Baker Jr., *Eur. J. Med. Chem.* **2012**, *47*, 560.

[26] a) H. Schäfer, C. Hess, H. Tobergte, A. Volf, S. Ichilmann, H. Eickmeier, B. Voss, N. Kashaev, J. Nordmann, W. Akram, B. Hartmann-Azanza, M. Steinhart, *Small* **2015**, *11*, 931; b) H. Schäfer, P. Ptacek, H. Eickmeier, M. Haase, *Adv. Funct. Mater.* **2009**, *19*, 3091.

[27] F. J. Arriagada, K. Osseo-Asare, *J. Colloid Interface Sci.* **1999**, *211*, 210.

[28] F. Chen, S. Zhang, W. Bu, Y. Chen, Q. Xiao, J. Liu, H. Xing, L. Zhou, W. Peng, J. Shi, *Chem. - Eur. J.* **2012**, *18*, 7082.

[29] S. Schietinger, L. d. S. Menezes, B. Lauritzen, O. Benson, *Nano Lett.* **2009**, *9*, 2477.

[30] a) N. M. Idris, M. K. G. Jayakumar, A. Bansal, Y. Zhang, *Chem. Soc. Rev.* **2015**, *44*, 1449; b) X. Liu, M. Zheng, X. Kong, Y. Zhang, Q. Zeng, Z. Sun, W. J. Buma, H. Zhang, *Chem. Commun.* **2013**, *49*, 3224.

[31] J. W. Walker, J. A. McCray, G. P. Hess, *Biochemistry* **1986**, *25*, 1799.

[32] a) S. Impellizzeri, B. McCaughan, J. F. Callan, F. M. Raymo, *J. Am. Chem. Soc.* **2012**, *134*, 2276; b) A. V. Karginov, Y. Zou, D. Shirvanyants, P. Kota, N. V. Dokholyan, D. D. Young, K. M. Hahn, A. Deiters, *J. Am. Chem. Soc.* **2010**, *133*, 420; c) E. A. Lemke, D. Summerer, B. H. Geierstanger, S. M. Brittain, P. G. Schultz, *Nat. Chem. Biol.* **2007**, *3*, 769; d) G. Mayer, A. Heckel, *Angew. Chem. Int. Ed.* **2006**, *45*, 4900; e) P. T. Wong, S. K. Choi, *Chem. Rev.* **2015**, *115*, 3388; f) C. Bao, L. Zhu, Q. Lin, H. Tian, *Adv. Mater.* **2015**, *27*, 1647.

[33] L. Bildstein, C. Dubernet, P. Couvreur, *Adv. Drug Delivery Rev.* **2011**, *63*, 3.

[34] a) S. K. Choi, T. P. Thomas, M.-H. Li, A. Desai, A. Kotlyar, J. R. Baker, *Photochem. Photobiol. Sci.* **2012**, *11*, 653; b) S. K. Choi, M. Verma, J. Silpe, R. E. Moody, K. Tang, J. J. Hanson, J. R. Baker Jr., *Bioorg. Med. Chem.* **2012**, *20*, 1281.

[35] M. A. Inlay, V. Choe, S. Bharathi, N. B. Fernhoff, J. R. Baker Jr., I. L. Weissman, S. K. Choi, *Chem. Commun.* **2013**, *49*, 4971.

[36] D. G. Mullen, M. Fang, A. Desai, J. R. Baker Jr., B. G. Orr, M. M. Banaszak Holl, *ACS Nano* **2010**, *4*, 657.

[37] a) S. K. Choi, A. Myc, J. E. Silpe, M. Sumit, P. T. Wong, K. McCarthy, A. M. Desai, T. P. Thomas, A. Kotlyar, M. M. Banaszak Holl, B. G. Orr, J. R. Baker, *ACS Nano* **2013**, *7*, 214; b) J. Rao, L. Yan, B. Xu, G. M. Whitesides, *J. Am. Chem. Soc.* **1999**, *121*, 2629.

[38] a) N. Parker, M. J. Turk, E. Westrick, J. D. Lewis, P. S. Low, C. P. Leamon, *Anal. Biochem.* **2005**, *338*, 284; b) S. D. Weitman, R. H. Lark, L. R. Coney, D. W. Fort, V. Frasca, V. R. Zurawski, B. A. Kamen, *Cancer Res.* **1992**, *52*, 3396.

[39] N. J. de Mol, M. J. E. Fischer, *Handbook of Surface Plasmon Resonance*, Vol. *5*, The Royal Society of Chemistry, Cambridge, UK, **2008**, p. 123.

[40] W. S. Hlavacek, R. G. Posner, A. S. Perelson, *Biophys. J.* **1999**, *76*, 3031.

[41] a) R. R. Anderson, J. A. Parrish, *J. Invest. Dermatol.* **1981**, *77*, 13; b) L. Fodor, M. Elman, Y. Ullmann, *Aesthetic Applications of Intense Pulsed Light*, Springer-Verlag, London, **2011**, p. 11.